Rare earth elements sorption to iron oxyhydroxide: model development and application to groundwater

Haiyan Liu, Olivier Pourret, Huaming Guo, Jessica Bonhoure

Rare earth elements sorption to iron oxyhydroxide: model development and application to groundwater

Haiyan Liu[1, 2, 3], Olivier Pourret[3,*], Huaming Guo[1, 2], Jessica Bonhoure[3]

[1]State Key Laboratory of Biogeology and Environmental Geology, China University of Geosciences (Beijing), Beijing 100083, P.R. China

[2]MOE Key Laboratory of Groundwater Circulation & Environment Evolution & School of Water Resources and Environment, China University of Geosciences (Beijing), Beijing 100083, P.R. China

[3]UniLaSalle, HydrISE, *60026 Beauvais Cedex*, France

*Corresponding author: olivier.pourret@unilasalle.fr, tel. +33 3 44 06 89 79.

Abstract: Iron oxyhydroxides are among the most important colloids that control rare earth elements (REE) concentrations and transport in natural hydrosystems. In this study, REE surface complexation to iron oxyhydroxides ($Fe(OH)_3(a)$) was described by using the Donnan diffuse layer model and a two-site (i.e. $\equiv Fe^sOH$ and $\equiv Fe^wOH$) model. The specific surface area and pH of zero charge were fixed as 100000 m^2/mol and 8.0, respectively. The surface site density for weak and strong binding sites were fixed at 0.1 mol/mol Fe ($\equiv Fe^wOH$) and 0.001 mol/mol Fe ($\equiv Fe^sOH$) respectively. The two site types were used with $pK_{a1}^{int} = 7.29$ and $pK_{a2}^{int} = 8.93$. Using linear free energy relationship, the estimated equilibrium surface complexation constants (log K) increased from light REE (LREE) to heavy REE (HREE). Results of REE modeling calculation using the determined log K revealed a good fit of experimental data, showing an order of sorption on iron oxyhydroxides: HREE > MREE > LREE and preferential sorption of HREE at a lower pH. However, sorption edges only showed a slight change with ionic strength (0.1 to 0.7 mol/L) for the whole REE series. The generalized model was subsequently used to evaluate the impact of iron oxyhydroxides on REE speciation in groundwater. Application of the model to "model groundwater" showed that iron oxyhydroxide complexes of REE were significant in near neutral and weakly alkaline pH. This study contributes to putting forward a comprehensive database which would be useful for the application of surface complexation model to describe REE sorption by amorphous ferric hydroxides in nature.

45 Keywords: Rare earth elements; Iron oxyhydroxides; Sorption; Surface complexation
46 modeling; Groundwater

47

48 1. Introduction

49 The great interest in determining the distribution and abundance of rare earth
50 elements (REE) in aquatic systems has been shown by numerous research works
51 generated over the past decades (Goldberg et al., 1963; Henderson, 1984; Dia et al.,
52 2000; Tang and Johannesson, 2003; Gruau et al., 2004; Atwood, 2013; Noack et al.,
53 2014; Gaillardet et al., 2014; Davranche et al., 2017). The solution and mineral
54 properties of REE make them effectively robust proxies for low temperature
55 geochemical reactions. It is generally recognized that REE systematic chemical
56 properties usually lead to REE fractionation in geochemical systems (Henderson,
57 1984). REE form a coherent group and generally occur in the trivalent oxidation state.
58 The effective ionic radii of the REE decrease with increasing atomic number
59 (Shannon, 1976). This effect causes characteristic regular features of normalized REE
60 patterns defining the CHArge and RAdius-Controlled process, CHARAC (Bau,
61 1996). If a low temperature geochemical system is characterized by a CHARAC
62 patterns, REE of similar charge and radius should display a coherent behavior. This
63 property, however, is no longer observed when chemical processes are driven by an
64 external electronic configuration that produces a sub-partition (non-CHARAC
65 processes). The CHARAC attribution of REE should thus generate smooth, rather

than irregular patterns (excepting redox-related Ce anomaly), which may indicate non-CHARAC behavior. The apparent subdivision of La and the fourteen *4f* REE elements into four groups or tetrads (I: La to Nd; II: Nd to Gd; III: Gd to Ho; IV: Ho to Lu) is referred as the Tetrad effect and a M-type lanthanide tetrad effect (Bau, 1996) is defined when subdivided into four concave-upward segments. The M-type tetrad effect has been shown on patterns of apparent REE distribution coefficients between iron oxyhydroxides and aqueous solutions (Bau, 1996) and contrasts to the complimentary W-type in the aqueous phase. In aquatic geochemical systems, REE fractionation takes place through complexation to reactive surface organic (Tang and Johannesson, 2003) and inorganic (Byrne and Li, 1995) ligands as well as surface complexation to aquifer minerals (Tang and Johannesson, 2005; Pourret and Davranche, 2013).

Despite the significant efforts that have been made toward the study of REE solution complexation with a variety of inorganic anions (carbonate, hydroxide, sulfate, fluoride, and chloride) and organic ligands (Wood, 1990; Tang and Johannesson, 2003; Pourret et al., 2007; Pourret and Martinez, 2009; Pourret et al., 2010). Far less is understood concerning REE surface complexation behavior on mineral surfaces. To date, few studies have been dedicated to REE sorption onto mineral surfaces (De Carlo et al., 1998; Bau, 1999; Ohta and Kawabe, 2001; Quinn et al., 2007; Schijf and Marshall, 2011). Early laboratory study of REE sorption onto Fe oxides showed that the light rare earth elements (LREE) were preferentially removed from solution over the heavy rare earth elements (HREE) (Koeppenkastrop and De

Carlo, 1992), although only a single pH value (i.e. pH 7.8) was considered. More recently, REE sorption on Fe (oxy)hydroxides in the absence of competing complexing ligands was investigated over a range of pH 4.0 to 9.0, as well as an ionic strength (IS) range of 0 to 0.7 mol/L (Ohta and Kawabe, 2001; Quinn et al., 2006, 2007). Further works of Bau (1999) and Ohta and Kawabe (2001), not only revealed the influences of pH and IS on REE sorption behaviour, but, in particular, non-CHARAC REE behaviors, such as lanthanide tetrad effect, were documented. Results of these experiments showed that the HREE exhibited a greater affinity for the solid phase than the LREE. Results from field experiments under acidic pH (pH<5.0) further indicated that LREE were preferentially enriched by hydrous Fe(III) oxides (Verplanck et al., 2004). Even if Mn oxides and humic substance play significant roles (Tang and Johannesson, 2003; Nakada et al., 2013; Pourret and Tuduri, 2017); previously cited studies demonstrated that Fe-oxyhydroxides may also control REE fractionation and partitioning in the natural environment.

However, although amorphous iron oxyhydroxides (e.g. $Fe(OH)_3(a)$) appear to be a most frequently studied solid for investigation of REE sorption, only a few works have accounted for this substrate (De Carlo et al., 1998; Bau, 1999; Ohta and Kawabe, 2001; Quinn et al., 2006). Poorly crystallized amorphous iron oxyhydroxides have a larger surface area and smaller site density than their crystalline counterparts (Henmi et al., 1980; Jambor and Dutrizac, 1998). This is evidenced by more extensive sorption of REE onto amorphous iron oxyhydroxides (Koeppenkastrop and De Carlo, 1992). The lack of data for REE binding by amorphous iron oxyhydroxides may be

attributed to the high variety of the equilibrium sorption constants, which complicates modeling studies. Such that, for example, the estimated REE partition coefficients ($_iK_{Fe}$) differ by a factor of approximately round 400 for individual REE binding constants at fixed pH (Schijf and Marshall, 2011). However, in order to more accurately predict REE behavior with respect to key environmental variables, such as pH and ionic strength, a quantitative description of REE binding to amorphous iron oxyhydroxides is urgently needed. Understanding of the fate and transport of REE is of importance regarding addressing health-related (e.g. liver function) (Zhu et al., 2007) and environmental issues (e.g. water pollution and farmland destruction) (Rim et al., 2013), due to the increasingly extensive use of REE in various aspects entailing an enhanced anthropogenic input (e.g. Gd anomaly) into environment (Bau and Dulski, 1996a; Verplanck et al., 2010).

In this study, a surface complexation model (SCM) was proposed to quantify REE sorption to amorphous iron oxyhydroxides. This SCM took into consideration the generic HFO surface parameters provided by Dzombak and Morel (1990). The REE-$Fe(OH)_3$(a) binding constants were extrapolated using the linear free energy relationship (LFER) methodology and were further validated by reproducing published experimental data within ionic strengths extending from of 0.1 to 0.7 mol/L, and a pH range of 4 to 9 (De Carlo et al., 1998). The model was developed for different IS and pH values (i.e. conditions of seawater and groundwater), and was eventually used to discuss the importance of iron oxyhydroxides REE sorption in natural groundwater.

2. Materials and methods

2.1. Surface complexation model description

The diffuse layer model is capable of describing the sorption of solutes onto hydrous oxides including those of iron, aluminum, manganese and silicon. As the central component of the generalized two-layer model, it has been used to compile a database of surface complexation reactions for hydrous ferric oxides (Dzombak and Morel, 1990), hydrous manganese oxides (Tonkin et al., 2004) and goethite (Mathur and Dzombak, 2006). The model is chosen principally because it is the simplest model which accounts qualitatively and quantitatively for all available sorption data for hydrous ferric oxides. Two binding sites, $\equiv Fe^{s}OH$ and $\equiv Fe^{w}OH$, (strong- and weak-affinity sites, respectively) were used in this SCM to describe sorption reactions with specific hydroxyl sites on the oxide surfaces. Surface equilibrium reactions (Eqs. (1) to (6)) are written as a combination of chemical free energy terms. The coulombic term represents the electrochemical sorption processes. This parameter was calculated from the Gouy-chapman electrical double layer theory, which considersed a surface charge layer and a diffuse layer of counter charges.

$$P=\exp(-F\psi/RT)$$

where F stands for the molar Faraday constant (96485 C/mol); R is molar gas constant (8.314 J/mol); T is the absolute temperature (K), and ψ is the electrostatic potential.

$$\equiv Fe^{w,s}OH^{o} + H+ = \equiv Fe^{w,s}OH_2^{+} \qquad K_{a1\equiv Fe^{w,s}OH} \qquad (1)$$

$$\equiv Fe^{w,s}OH^{o} = \equiv Fe^{w,s}O^{-} + H^{+} \qquad K_{a2\equiv Fe^{w,s}OH} \qquad (2)$$

$$\equiv Fe^{w}OH^{o} + M^{n+} = \equiv Fe^{w}OM^{(n-1)+} + H^{+} \qquad K_{\equiv Fe^{w}OM} \qquad (3)$$

$$\equiv Fe^{w}OH^{o} + M^{n+} + H_2O = \equiv Fe^{w}OMOH^{(n-2)+} + 2H^{+} \qquad K_{\equiv Fe^{w}OMOH} \qquad (4)$$

$$\equiv Fe^{s}OH^{o} + M^{n+} = \equiv Fe^{s}OM^{(n-1)+} + H^{+} \qquad K_{\equiv Fe^{s}OM} \qquad (5)$$

$$\equiv Fe^{s}OH^{o} + M^{n+} + H_2O = \equiv Fe^{s}OMOH^{(n-2)+} + 2H^{+} \qquad K_{\equiv Fe^{s}OMOH} \qquad (6)$$

Acidity constants (pK_{a1} and pK_{a2}) for iron oxyhydroxides, presented in Table 1, were obtained from Dzombak and Morel (1990). Specific surface area (SSA) and site density values required for the SCM model were those proposed by Parkhurst and Appelo (2013). Total concentrations of surface sites (i.e. surface site densities) were divided into strong and weak affinity fractions for REE binding (Table 1). Therefore, REE sorption onto oxide surfaces was simulated by assuming two binding sites. It should be noted that the site density can range from 0.001 to 0.1 mol/mol Fe, and from 0.1 to 0.3 mol/mol Fe for strong and weak binding sites, respectively, due to different estimation methods (Dzombak and Morel, 1990). A generic site density value (0.001 mol/mol Fe and 0.1 mol/mol Fe fraction for strong and weak binding sites, respectively) was chosen for $Fe(OH)_3(a)$ in the present model, following the suggestion of Parkhurst and Appelo (2013). Modeling calculations were performed using the hydrogeochemical code PHREEQC version 3.3.9 (Parkhurst and Appelo, 2013), following the method described by Pourret and Davranche (2013). The input Fe(III) was considered to precipitate as $Fe(OH)_3(a)$ instantaneously with an equilibrium constant log K=4.89 (Nordstrom et al., 1990). The amounts of the binding sites for these two-type of sites were determined by the amount of $Fe(OH)_3(a)$. The

169 $Fe(OH)_3$(a) was defined explicitly in keyword data block EQUILIBRIUM PHASES.
170 The SSA was defined relative to the moles of $Fe(OH)_3$(a), in which the amount of
171 specified binding sites changed as the SSA varied during batch-reaction simulation.
172 Upon $Fe(OH)_3$(a) precipitation, the two types of oxide surface binding sites ($\equiv Fe^{s}OH$
173 and $\equiv Fe^{w}OH$) were assumed to be available for REE complexation. For SCM
174 modeling, surface-complexed and diffuse layer species, were taken as the components
175 of the system. REE surface complexation modeling was then performed in the
176 presence of iron oxyhydroxides. Following the method described in Hummel et al.
177 (2002) activity coefficients were calculated using the Davies (1962) approach.

178 2.2 Estimation of the REE-$Fe(OH)_3$(a) stability constants

179 Surface complexation constants were estimated using linear free energy
180 relationship (LFER) by the method of Pourret and Davranche (2013), and as shown
181 previously (Schindler et al., 1976; Dzombak and Morel, 1990; Tang and Johannesson,
182 2003; Tonkin et al., 2004; Mathur and Dzombak, 2006; Pourret et al., 2007).
183 Specifically, due to the similarity of surface complexation for metal ions to the
184 corresponding hydrolysis reaction in solution, the energy of metal ion complexation
185 with hydroxyl ions in solution could be correlated with that of the binding of metal
186 ions to deprotonated surface hydroxyl groups. Therefore, the first hydrolysis constants
187 could be correlated with surface complexation constants (Mathur and Dzombak, 2006;
188 Schott et al., 2009). As such, REE surface complexation constants could be obtained
189 by extrapolation of aqueous hydrolysis reactions. The metal ion (including Ag^{+}, Co^{2+},
190 Ni^{+}, Cd^{2+}, Zn^{2+}, Cu^{2+}, Pb^{2+}, Hg^{2+}) complexation reaction parameters that were used for

verifying the fit of REE sorption data to iron oxyhydroxides were obtained from Dzombak and Morel (1990). The solution complexation reactions for these metals could be defined similarly to Eqs. (3) to (6). The LFER for metal cations was defined by the log $K_{\equiv Fe^{s}OM}$, log $K_{\equiv Fe^{s}OMOH}$, log $K_{\equiv Fe^{w}OM}$ and log $K_{\equiv Fe^{w}OMOH}$ and the hydrolysis (OH) constants. The correlation of log K with the first hydrolysis constant log K_{MOH} for these metal ions was given by equations (7) to (10). The REE first hydrolysis constant (log K_{LnOH}) (Table 2) was obtained from Klungness and Byrne (2000) and was used for subsequent extrapolation of REE stability constants.

$$\text{Log } K_{\equiv Fe^{s}OM} = 1.17 \log K_{MOH} - 7.89 \quad (7)$$

$$\text{Log } K_{\equiv Fe^{s}OMOH} = 0.79 \log K_{MOH} - 7.69 \quad (8)$$

$$\text{Log } K_{\equiv Fe^{w}OM} = 1.30 \log K_{MOH} - 7.89 \quad (9)$$

$$\text{Log } K_{\equiv Fe^{w}OMOH} = 1.97 \log K_{MOH} - 16.56 \quad (10)$$

The extrapolated REE stability constants are shown in Table 2. Only the equilibrium stability constants $\log K_{\equiv Fe^{s}OLn}$ and $\log K_{\equiv Fe^{w}OLn}$ were considered as the amount of the REE binding through the reactions in Eqs. (4) and (6), with $\log K_{\equiv Fe^{s}OLnOH}$ and $\log K_{\equiv Fe^{w}OLnOH}$, was negligible.

Experimental REE data from literature (De Carlo et al., 1998) was subsequently used to validate the equilibrium surface complexation constants for the whole REE series in a reactor open to the atmosphere and at room temperature, in the presence of a $[Ln^{n+}]$ of 125 μg/L for each of the 14 REE; [Fe(III)] = 10 mg/L; and an IS range of 0.1 to 0.7 mol/L $NaNO_3$. REE carbonate species were not considered in this study,

208 although De Carlo et al.'s (1998) experiment showed an influence of REE solution
209 complexation with CO_3^{2-}. Modeling calculations were carried out with the Nagra/PSI
210 database (Hummel et al., 2002). This database has been updated by the incorporation
211 of the well-accepted stability constants at zero ionic strength and 25 ºC for REE
212 inorganic anion complexation including: (1) chloride ($LnCl^{2+}$, $LnCl_2^{+}$) (Luo and
213 Byrne, 2001), (2) fluoride (LnF^{2+}) (Luo and Millero, 2004), (3) sulfate ($LnSO_4^{+}$)
214 (Schijf and Byrne, 2004), (4) nitrate ($LnNO_3^{2+}$) (Millero, 1992), (4) hydroxide
215 ($LnOH^{2+}$, $Ln(OH)_2^{+}$, $Ln(OH)_3$(a)) (Lee and Byrne, 1992; Klungness and Byrne,
216 2000), (5) carbonate ($LnCO_3^{+}$ and $Ln(CO_3)_2^{-}$) (Luo and Byrne, 2004). The specific
217 log K values are presented in the supplementary information (Table S1). It should be
218 pointed out that, to be consistent with the experimental settings (De Carlo et al., 1998),
219 binding of the first hydrolysis species $LnOH^{2+}$ and carbonate ions onto iron
220 oxyhydroxides was not included in our simulations. All the REEs considered in the
221 model in this study were trivalent, because oxidation of REEs like Ce(III) should
222 occur after initial sorption onto mineral surface sites (Bau, 1999).

223 **3. Results and discussion**

224 3.1 REE-$Fe(OH)_3$(a) modeling with extrapolated stability constant

225 3.1.1 Modeling of REE complexation to iron oxyhydroxides

226 To test the validity of the extrapolated stability constants and the diffuse layer
227 SCM, calculations herein were performed using data obtained from literature under
228 the conditions described by De Carlo et al. (1998). The modeling results in this study

were compared to REE sorption experimental data recorded previously (De Carlo et al., 1998). As sorption behavior of the fourteen REE members were similar, subsequent results and discussions focus on La, Ce, Eu and Lu. Lanthanum, Eu and Lu represent light REE (LREE), middle REE (MREE), and heavy REE (HREE), respectively. Cerium was selected to highlight the peculiar behavior of the only redox sensitive lanthanide in the experimental conditions. As shown in figure 1, the calculated proportions of bound REE (i.e. La, Ce, Eu and Lu) increased with increasing pH (3 to 9). Relatively higher sorptive proportions were modeled with IS of 0.1 as compared to those of 0.3 and 0.7. for all REEs and pH region (Fig. 1). These results are consistent with experimental data sets therein (De Carlo et al., 1998), especially for LREE (Figs. 1a and b). For MREE (illustrated by Eu) and HREE (illustrated by Lu), however, although a relatively higher binding strength was predicted by the model under increasing pH (Fig. 1c and d), the model fit results were in agreement with experimental data within the pH range of 4 to 6.5. The discrepancy between modeled and experimental data, seemed to become significant with increasing pH and IS, and REE atomic number. The difference between modeled and experimental data was lower for LREE (e.g. less than 10% for La and Ce) than for MREE and HREE (between 20 and 30% for Eu and Lu, respectively). This may be attributed to REE carbonate complexation or to the presence of more than two binding sites on the mineral surfaces which were not accounted by the LFER model in De Carlo et al. (1998). Previous studies demonstrated that REE binding by carbonate in solution increased with REE atomic number (Lee and Byrne, 1992). Indeed, REE

carbonate complexation in solution was stronger than sorption of the HREE onto oxide surfaces (i.e. FeOOH and δ-MnO_2) when compared to the LREE (Koeppenkastrop and De Carlo, 1993). Kawabe et al. (1999) have examined the effect of REE carbonate complexation on REE sorption onto Fe oxyhydroxides. Their results further showed that distribution coefficients (K_d, commonly used in estimating the potential sorption of dissolved metals by a solid phase, Fe oxyhydroxide in our case) increased with the atomic number in carbonate-free system, whereas K_d declined across the REE series more significantly for HREE in the presence of carbonate. Therefore, the discrepancy observed in sorption between the HREE and the LREE indicated that larger concentrations of HREE were predicted to be sorbed by present model, which have not considered carbonate species, than those under the experimental conditions.

3.1.2 Effect of pH on REE sorption behavior

To a first approximation, REE sorption patterns displayed a similar behavior to that of trace-metal cations. As the pH becomes more alkaline, metal sorption onto reactive solids (e.g. iron oxyhydroxides) increased from 0 to 100% over a narrow pH range (Dzombak and Morel, 1990). Figure 1 showed that 5% of the LREE (i.e. La and Ce) were sorbed at pH<6.0, and >70% at pH=8.0 (i.e. 70% to 80% for La; 88% to 93% for Ce), whereas, sorbed fractions of MREE and HREE (i.e. Eu and Lu, respectively) ranged from about 10% at pH= 6.0 to near 100% at pH=8.0. This demonstrated pH edges shifted to lower values for HREE and MREE with respect to LREE. Therefore, the model fit suggested a preferential sorption of HREE and MREE

relative to LREE. HREE and MREE began to be sorbed at a lower pH than LREE (Fig. 2). Such that, under IS=0.1mol/L condition, sorption of Lu triggered at pH around 4, while Eu and La at pH 5 and 6, respectively (Fig. 2a). The similar characteristic was observed at IS=0.3 mol/L (Fig. 2b) and IS=0.7 mol/L (Fig. 2c), as well as has already been highlighted in De Carlo et al. (1998) and observed in Bau (1999). Indeed, when the amount of Fe(III) concentration in the SCM was decreased, the fractional sorption at a given pH was reduced (Fig. 3). In order for the proportion of sorbed REE to remain fixed as it was at low sorbent condition, pH edges shifted to the right. However, the shift appeared to be more pronounced for LREE than MREE and HREE (Fig. 3). Specifically, the pH where 50% of the total REE was sorbed, increases from 7.2 to 7.8, and from 6.2 to 6.5, and from 5.7 to 5.9 for La, Eu, Lu, respectively, when the Fe(III) input decreased by 50%. This was further evidenced for the more efficiency of sorption of HREE and MREE at lower pH as compared to LREE.

3.1.3 REE partitioning and fractionation

The distribution and fractionation of the REE sorbed by iron oxyhydroxides (at IS = 0.5 mol/L and within a pH range of 5.5-8.0) were further modeled using the SCM procedure described above. Figure 4 shows the proportion of sorbed REE as a function of REE atomic number. To further evaluate REE fractionation, Yb/Gd and La/Sm ratios were considered to fully quantify HREE and LREE enrichment, respectively. Calculated REE patterns showed HREE enrichments ($\%Yb_{sorb}/\%Gd_{sorb}$ ranging between 1.1 and 5.4; if $\%Yb_{sorb}/\%Gd_{sorb}>1$, REE patterns highlight HREE

enrichment, and vice versa) and LREE depletion ($\%La_{sorb}/\%Sm_{sorb}$ ranging between 0.08 and 0.91; if $\%La_{sorb}/\%Sm_{sorb}<1$, REE patterns feature LREE enrichment, and vice versa). Most importantly, this patterns exhibited (i) concave-upward Tetrad effect with tetrads ranging from 1.00 to 1.32 (using the method proposed by Irber (1999)) and (ii) positive Ce anomalies ($Ce/Ce^*=\%Ce_{sorb}/(\%La_{sorb}\times\%Pr_{sorb})^{0.5}$) with Ce/Ce* ranging from 1.01 to 1.74 (average 1.54)) (Fig. 4). These features contrasted with CHARAC REE patterns and strongly suggested that REE complexation behavior was additionally controlled by their electron configuration and the complexing hydroxyl group on the oxide surface, rather than by the REE ionic charge and radius (Bau, 1996). The REE fractionation patterns also coincided with SCM predictions, indicating that the HREE had a stronger affinity for iron oxyhydroxides than the LREE. Moreover, Ce was preferentially enriched on the iron oxyhydroxide surface relative to neighboring La and Pr. The results are in good agreement with the experimental datasets provided by Bau (1999) and Ohta and Kawabe (2001). At the IS of 0.5 mol/L, Schijf and Marshall (2011) calculated REE distribution coefficients on hydrous ferric oxides over the pH range 3.9-8.4. Their calculated REE patterns, however, showed a less pronounced tetrad effect and no apparent positive Ce anomalies. This is because of the weaker, and less pH dependent sorption of the REE on iron oxyhydroxides, under their experimental conditions (Schijf and Marshall, 2011). However, the results from Verplanck et al. (2004) are strikingly similar to those obtained in this study. The authors employed a lower pH (i.e. pH<5.1) to model REE partitioning relative to De Carlo et al. (1998) and Schijf and Marshall (2011).

317 The calculated complexation of REE with hydrous ferric oxides by Verplanck et al.
318 (2004) showed a convex Tetrad curve and a positive Ce anomaly, as shown in Fig. 4.
319 Moreover, the HREE fractionated more significantly with respect to the LREE in their
320 study (i.e. Yb_n/Gd_n ranging from 4.3 to 7.1; for further information see Verplanck et
321 al. (2004)). This further indicates that REE partitioning and fractionation on iron
322 oxyhydroxides are more influenced by low pH conditions. The upward Tetrad effect
323 curves were more apparent at acidic pH values (Fig. 4a). Indeed, as the pH decreased,
324 enhanced protonation of ferric oxides surface occurs, leading to a decrease in the
325 proportion of negatively charged groups being able to complex REE (Bethke, 2007).
326 One of the most striking features of the modeling results in this study was that
327 Ce was preferentially sorbed by iron oxyhydroxides from the solution, with respect to
328 La and Pr, at acidic pH (Fig. 4). The positive Ce anomaly began to decrease at a pH of
329 6, which may be due to a global increase of neighboring REE, since REE sorption
330 increases as the pH rises above 6 (up to 100%). Therefore, the Ce sorption edge in
331 iron oxyhydroxides was below pH 5, and lower than that of La. Although positive Ce
332 anomaly may result from anomalous La enrichment, as interpreted by Bau and Dulski
333 (1996b), further calculations showed that the observed accumulated Ce was not
334 interfered by La (supplementary information Fig. S2). It should be noted that in
335 low-temperature aquatic systems, Ce is the only REE that can occur in a stable
336 tetravalent state (i.e. as Ce(IV)). This can be explained by the oxidation scavenging of
337 Ce(III) from aqueous onto metal oxide surfaces, which leads to a decoupling of Ce
338 from its neighbors, La and Pr (Bau, 1999). Nevertheless, sorption experiments

described by Nakada et al. (2013) showed that the sorbed Ce on ferrihydrite might not have been oxidized in the Ce/ferrihydrite system, which was evidenced by XANES analysis and the thermodynamic data. In consequence, although the redox properties of Ce(III) were not taken into account for REE modeling calculations in this study, the estimated REE sorption dataset are able to provide a better understanding of the mechanism of preferential accumulation of the Ce onto the iron oxyhydroxide surfaces.

3.2 Model validity and application

3.2.1 SCM of REE sorption to iron oxyhydroxides

In order to check the validity of the SCM of REE sorption to iron oxyhydroxides, additional calculations were performed using literature data from field studies (Pourret et al., 2010; Guo et al., 2010; Liu et al., 2016). Sampling location of the modeled groundwater extends from the recharge zone to discharge areas, which considers the variable aqueous chemistry (including pH, IS, ∑REE and Fe(III) concentrations) over a flow system. The considered pH ranges from 6.70 to 8.32, the metal loading (∑REE) from 0.20 μg/L to 4.25 μg/L and the dissolved Fe(III) from 19.6 μg/L to 740 μg/L. As shown in Fig. 5, the results from surface complexation modeling of the field data were similar to those obtained for the experimental data of De Carlo et al. (1998), showing an upward tetrad effect REE pattern and positive Ce anomalies (Ce/Ce* ranging from 1.13 to 1.61 (average 1.50)). This has been observed, in spite of the lower IS (e.g. 0.006 < IS < 0.019 mol/L) for these field samples with

360 respect to solutions used in De Carlo et al. (1998), as well as in Ohta and Kawabe
361 (2001) and Bau (1999). In addition to the IS, a lower metal loading was observed with
362 respect to the experimental conditions (e.g. 4.25 µg/L for Pourret et al. (2010); 0.21
363 µg/L for Guo et al. (2010)). The stronger REE binding (e.g. total sorbed REE ranging
364 from 39% to 51%) for the Guo et al.'s (2010) sample resulted from the higher ferric
365 oxide content and higher pH. However, under these conditions, the fractionation
366 between individual REE occurred to a lesser extent (Fig. 5). As $\%Yb_{sorb}/\%Gd_{sorb}$ (i.e.
367 0.80) and $\%La_{sorb}/\%Sm_{sorb}$ (i.e. 1.04) ratios were close to 1, REE patterns tended to be
368 flat. Eventually, modeling results are coherent with ultrafiltration experiments
369 performed on sample PG3 (Pourret et al., 2010) which highlighted that large colloids
370 comprising Fe oxides (>30 kDa) only controlled a small fraction of REE.

371 Apart from these discrepancies, the inclusion of carbonate species can be the
372 major difference between the modeling and field studies. While CO_2 species were not
373 considered in the modeling as shown in De Carlo et al.'s (2010), carbonate ligands are
374 strong complexing agents for aqueous HREE at alkaline pH (Johannesson et al., 1996;
375 Luo and Byrne, 2004). This may explain that a slightly higher sorption of the HREE
376 by iron oxyhydroxides was calculated at alkaline pH by the model fit with respect to
377 experimental data (Fig. 1d). When field samples were used (HCO_3^- ranging from 322
378 to 501 mg/L) for further modeling (Fig. 5), the calculated REE patterns changed to be
379 less enriched in HREE (e.g., when pH increases), as evidenced by the generally
380 lower $\%Yb_{sorb}/\%Gd_{sorb}$ ratios (1.04 to 2.32). However, these ratios were within the
381 range of the De Carlo et al.'s (1998) modeling of experimental datasets, as shown

above (Fig. 4). To be more specific, REE species including Fe-oxyhydroxide complexes as function of atomic number are shown in Fig. 6. In the modeled groundwater of low Fe(III) concentration, REE chiefly occurred as carbonate complexes ($LnCO_3^+$ and $Ln(CO_3)_2^-$) (Fig. 6a and b), whereas as Fe(III) concentration increased, more REE were complexed with iron oxyhydroxides and carbonate ligands became the primarily competitor (Fig. 6c). The other REE species (including Ln^{3+}, $LaSO_4^+$, $LnOH^{2+}$ and $Ln(OH)_2^+$) were not significant, although free metal ion (Ln^{3+}) had proportion greater than 10% for La and Ce in low pH groundwaters (Fig. 6a, b and c). This was best observed for Guo et al's (2010) groundwater (Fig. 6d), where dicarbonato complex ($Ln(CO_3)_2^-$) dominated the remaining aqueous REE and its proportion increased from LREE (i.e., La 22%) to HREE (i.e., Lu 48%). An increasing trend for Fe-oxyhydroxide complex fraction with increasing REE atomic number was also observed in Guo et al's (2010) sample (i.e., increasing from 38% for La to 47% for Lu) (Fig. 6d). This was attributed to the higher Fe(III) concentration and higher pH as compared to the other three samples. Therefore, although SCM estimated stability constants may be dependent on IS, pH, Fe(III) concentration and metal loading, the unique attributes of the REE series are useful for examining whole log K patterns. Furthermore, combine the well-accepted inorganic anion complexation with the SCM, the model is able to highlight the REE partitioning and fractionation between solution and iron oxide surfaces, as already highlighted in Fig. 6.

In particular, insight can be gained from SCM to understand lanthanide tetrad effect generated from REE sorption onto iron oxyhydroxide surfaces. Calculation of

404 the four tetrads following the method described by Irber (1999) showed that the value
405 increases from the first tetrad (t_1) to the fourth tetrad (t_4) ($1.10 \leq T \leq 1.45$ for PG3
406 (Pourret et al., 2010); $1.01 \leq T \leq 1.05$ for No. well 48 (Guo et al., 2010);
407 $1.09 \leq T_{average} \leq 1.28$ for Liu et al. (2016); $T = t_1 + t_2 + t_3 + t_4$). Moreover, the calculated
408 tetrad values decreased with increasing pH. This has been featured in Figure 5. This
409 aqueous-solid (i.e. iron oxyhydroxide) reaction has been considered as one of the
410 most important processes responsible for the non-CHARAC REE behavior and REE
411 abundance in aqueous solutions (Koeppenkastrop and De Carlo, 1992, 1993; Bau,
412 1996, 1999; Schijf and Marshallv, 2011; Verplanck et al., 2004). In addition to the
413 tetrad effect, the modeling approach reproduced the stronger sorption proportion of
414 Ce with respect to neighbors La and Pr. This was further evidenced by the largest
415 positive Ce anomaly (Ce/Ce* 1.61) observed by Pourret et al. (2010) and lowest
416 positive Ce anomaly (Ce/Ce* 1.13) in Guo et al. (2010). This may account in part for
417 the negative Ce anomalies for normalized REE patterns in these field groundwater
418 samples (0.58 for Pourret et al. (2010); 0.39 for Guo et al. (2010); average 0.94 for
419 Liu et al. (2016)). The non-CHARAC (e.g. lanthanide tetrad effect) REE behavior and
420 negative Ce anomaly are widely observed in natural waters (Elderfield et al., 1990;
421 Bau, 1996). These are, for the most part, attributed to the surface complexation of the
422 REE by iron oxyhydroxides. The complexation is, however, not only exclusively
423 dependent on REE ionic charge and radius, but controlled by variations in the electron
424 configurations of REE and by the type of complexing ligands. Furthermore, the model
425 also suggests that the contribution of REE scavenging of iron oxyhydroxides towards

426 the lanthanide tetrad effect and the removal of Ce from solution should be most
427 significant at acidic pH.

428 3.2.2 REE speciation calculation for world average groundwater

429 The developed model was used to evaluate REE speciation for world average
430 groundwater, proposed as "model groundwater" by Tang and Johannesson (2003).
431 The concentrations of major anions and REE for world average groundwater used in
432 the model were obtained from Wood (1990), whereas the concentrations of cations
433 and Fe were taken from Livingstone (1963). These parameters have been previously
434 used by Lee and Byrne (1992), Johannesson et al. (1996) and Tang and Johannesson
435 (2003) for investigation of REE complexation behavior in groundwater. Thus REE
436 speciation calculation was performed keeping the solute compositions constant and
437 changing pH. The dissolved ligands (i.e. carbonates, sulfates, hydroxyls) present in
438 the modeled groundwater are similar to those considered by Wood (1990) at pH=7
439 and 20 °C (calculating using PHREEQC).

440 The results of these calculations for La, Eu and Lu are shown in Fig. 7. It is
441 obviously observed from Fig. 7a, b and c, in the "model groundwater" with Fe(III)
442 concentrations of 0.672 mg/L, the SCM predicted that REE: (i) occurred
443 predominately as free metal ion (Ln^{3+}) and sulfate complex ($LnSO_4^+$) at pH between 4
444 and 6.5; (ii) were significantly associated with Fe oxide (Hfo_oLn^{2+}) at pH between
445 6.5 and 8; (iii) chiefly as carbonate complex ($LnCO_3^+$ and $Ln(CO_3)_2^-$) at pH between 8
446 and 9.5, and (iv) were dominated by hydroxide complex ($LnOH^{2+}$ and $Ln(OH)_2^+$) at
447 pH above 9.5; (v) negligibly as chloride complex ($LnCl^{2+}$ and $LnCl_2^+$) and nitrate

448 complex ($LnNO_3^{2+}$) (below 1%) in the pH range. Generally speaking, the modeling
449 results for acidic and alkaline groundwaters were in good agreement with previous
450 investigations of natural groundwater (Wood, 1990; Lee and Byrne, 1992;
451 Johannesson, 2005). It should be noted, however, that these earlier studies did not
452 consider REE complexation with iron oxyhydroxides. The accordance of the present
453 SCM with previously purely inorganic speciation models for acid and alkaline
454 groundwaters should thus be verified by further field or laboratory investigations in
455 these pH conditions. However, it is also worth noting that the predominant
456 characteristic for the modeling calculations is that significant amounts of REE are
457 complexed with iron oxyhydroxide for groundwaters of near neutral and weakly
458 alkaline pH. Indeed, the model predicted that 20% to 30% of LREE (i.e. La) occurred
459 as iron-oxyhydroxide complexes (Hfo_OLa^{2+}) in the pH range from 7.5 to 9.0 (Fig.
460 7a), whereas for MREE (i.e. Eu) and HREE (i.e. Lu), 20% to 50% (Hfo_OEu^{2+}) and
461 20% to 80% (Hfo_OLu^{2+}) were complexed with iron-oxyhydroxide in the pH ranges
462 from 6.5 to 9.0, and from 6.3 to 9.0, respectively. Furthermore, a strong competition
463 between REE surface complexation and solution complexation has also been observed
464 in the model, and that the competition changes with pH (Fig. 7). In particular, REE
465 carbonate complexes ($LnCO_3^+$ and $Ln(CO_3)_2^-$) were the most important inorganic
466 ligands competing with iron oxyhydroxide in near neutral and weakly alkaline
467 groundwaters, and thus this process was responsible for the mobility and transport of
468 REE in natural groundwater systems. This is well consistent with the modeling results
469 using field sampled groundwater, as discussed above (Fig. 6). In this model, the

influences of organic matter and manganese oxyhydroxides on REE speciation were not taken in account, although previously researches demonstrated they could played an important role in REE behavior (Tang and Johannesson, 2003; Nakada et al., 2013; Pourret et al., 2009; Pourret and Tuduri 2017). However, as was the case documented by Verplanck et al. (2004) and Quinn et al. (2007), the generalized proposed model is able to provide important suggestion for REE complexation with iron oxyhydroxides in Fe-rich groundwater-aquifer systems, unless other potential complexers (e.g. manganese or humics) are essentially present in aquifers and complex the REE.

4. Conclusion

Surface complexation modeling with high and low affinity sites was used to test REE sorption onto iron oxyhydroxides by considering a LFER to determine log K values. The extrapolated equilibrium surface complexation constants were further validated by using them to fit various experimental data sets (De Carlo et al., 1998). Results of SCM using the determined constants showed that the role of iron oxyhydroxide in complexing REE exhibited dependence upon pH, IS and the concentration of iron oxyhydroxide. The proportion of iron oxyhydroxide complexes showed upward lanthanide tetrad effect patterns as a function of atomic number, with stronger sorption of Ce than neighboring La and Pr over a wide variety of conditions (i.e. pH from 4.0 to 9.0; IS from 0 to 0.7 mol/L; [REE] from 0.14 μg/L to 125 μg/L; [Fe(III)] ranging from 0.0183 mg/L to 10 mg/L). Speciation calculations using the SCM suggest that iron oxyhydroxides are important complexers of REEs in groundwaters, and they effectively compete with dissolved inorganic ligands under

492 various conditions. For the first time, the generalized proposed model allows us to
493 predict the impact of iron oxyhydroxides on REE in natural environment. Compared
494 to previous modeling studies (e.g. Verplanck et al. (2004) and Schijf and Marshall
495 (2011)), this type of SCM accounts for a wider range of pH and IS, and particularly
496 can be a good application to natural groundwater. Furthermore, the increase of the
497 determined constants with increasing atomic number provides insight into
498 understanding of the discrepancy for HREE between modeled and experimental data.
499 Further development of the modeling techniques should incorporate Mn oxides,
500 humic substances and Fe oxides simultaneously into model, in order to obtain a
501 comprehensive model, and to better understand the roles of particle colloids in REE
502 mobility in natural systems.

503 **Acknowledgement**

504 We would like to acknowledge China Scholarship Council (CSC) for sponsoring
505 the first author's study in France (CSC No. 201606400016). We thank Dr. Raul E.
506 Martinez for comments on an early draft and post-editing the English style.

507 **References**

508 Atwood, D.A. 2013. The rare earth elements: fundamentals and applications. John
509 Wiley & Sons. pp.1-19.
510 Bau, M., Dulski, P. 1996a. Distribution of yttrium and rare-earth elements in the
511 Penge and Kuruman iron-formations, Transvaal Supergroup, South
512 Africa. Precambrian Research, 79(1-2), 37-55.
513 Bau, M., Dulski, P., 1996b. Anthropogenic origin of positive gadolinium anomalies in
514 river waters. Earth and Planetary Science Letters, 143, 245-255.

Bau, M. 1996. Controls on the fractionation of isovalent trace elements in magmatic and aqueous systems: evidence from Y/Ho, Zr/Hf, and lanthanide tetrad effect. Contributions to Mineralogy and Petrology, 123(3), 323-333.

Bau, M. 1999. Scavenging of dissolved yttrium and rare earths by precipitating iron oxyhydroxide: experimental evidence for Ce oxidation, Y-Ho fractionation, and lanthanide tetrad effect. Geochimica et Cosmochimica Acta, 63(1), 67-77.

Bethke, C.M. 2007. Geochemical and biogeochemical reaction modeling. Cambridge University Press. Second edition.

Byrne, R.H., Li, B. 1995. Comparative complexation behavior of the rare earths. Geochimica et Cosmochimica Acta, 59(22), 4575-4589.

Davies, C.W., 1962. Ion Association. Butterworths, London.

Davranche, M., Gruau, G., Dia, A., Le Coz-Bouhnik, M., Marsac, R., Pédrot, M., Pourret, O. 2017. Chapter 7. Rare Earth Elements in Wetlands. In Trace Elements in Waterlogged Soils and Sediments. Eds Rinklebe J., Knox A.S., Paller M.,Taylor & Francis Group/CRC Press, 135-162.

De Carlo, E.H., Wen, X.Y., Irving, M. 1998. The influence of redox reactions on the uptake of dissolved Ce by suspended Fe and Mn oxide particles. Aquatic Geochemistry 3, 357-389.

Dia, A., Gruau, G., Olivié-Lauquet, G., Riou, C., Molénat, J., Curmi, P. 2000. The distribution of rare earth elements in groundwaters: assessing the role of source-rock composition, redox changes and colloidal particles. Geochimica et Cosmochimica Acta, 64(24), 4131-4151.

Dzombak, D.A., Morel, F.M. 1990. Surface complexation modeling: hydrous ferric oxide. John Wiley & Sons.

Elderfield, H., Upstill-Goddard, R., Sholkovitz, E.R. 1990. The rare earth elements in rivers, estuaries, and coastal seas and their significance to the composition of ocean waters. Geochimica et Cosmochimica Acta, 54(4), 971-991.

Gaillardet, J., Viers, J. and Dupré, B. 2014. 7.7-Trace Elements in River Waters, in: Holland, H.D., Turekian, K.K. (Eds.), Treatise on Geochemistry (Second Edition). Elsevier, Oxford, pp. 195-235.

545 Goldberg, E.D., Koide, M., Schmitt,R.A., Smith, R.H. 1963. Rare-Earth distributions
546 in the marine environment. Journal of Geophysical Research, 68(14), 4209-4217.
547 Gruau, G., Dia, A., Olivie-Lauquet, G., Davranche, M., Pinay, G. 2004. Controls on
548 the distribution of rare earth elements in shallow groundwaters. Water
549 Research, 38(16), 3576-3586.
550 Guo, H.M., Zhang, B., Wang, G.C., Shen, Z.L., 2010. Geochemical controls on
551 arsenic and rare earth elements approximately along a groundwater flow path in
552 the shallow aquifer of the Hetao Basin, Inner Mongolia. Chemical Geology
553 270,117-125.
554 Henderson, P. 1984. Rare earth element geochemistry, Elsevier, Amsterdam.
555 Henmi, T., Wells, N., Childs, C.W., Parfitt, R.L. 1980. Poorly-ordered iron-rich
556 precipitates from springs and streams on andesitic volcanoes. Geochimica et
557 Cosmochimica Acta, 44(2), 365-372.
558 Hummel, W., Berner, U., Curti, E., Pearson, F.J., Thoenen, T. 2002. Nagra/PSI
559 chemical thermodynamic data base 01/01. Universal Publishers, Parkland,
560 Florida.
561 Irber, W. 1999. The lanthanide tetrad effect and its correlation with K/Rb, Eu/Eu∗ ,
562 Sr/Eu, Y/Ho, and Zr/Hf of evolving peraluminous granite suites. Geochimica et
563 Cosmochimica Acta, 63(3), 489-508.
564 Jambor, J.L., Dutrizac, J.E. 1998. Occurrence and constitution of natural and synthetic
565 ferrihydrite, a widespread iron oxyhydroxide. Chemical Reviews, 98(7),
566 2549-2586.
567 Johannesson, K.H., Stetzenbach, K.J., Hodge, V.F., Lyons, W.B. 1996. Rare earth
568 element complexation behavior in circumneutral pH groundwaters: assessing the
569 role of carbonate and phosphate ions. Earth and Planetary Science
570 Letters, 139(1-2), 305-319.
571 Johannesson, K.H., 2005. Rare earth elements in groundwater flow systems. Springer,
572 Dordrecht. Book. Water Science and Technology Library. Volume 51

573 Kawabe, I., Ohta, A., Miura, N. 1999. Distribution coefficients of REE between Fe
574 oxyhydroxide precipitates and NaCl solutions affected by REE-carbonate
575 complexation. Geochemical journal, 33(3), 181-197.
576 Klungness, G.D., Byrne, R.H., 2000. Comparative hydrolysis behavior of the rare
577 earths and yttrium: the influence of temperature and ionic strength. Polyhedron
578 19, 99-107.
579 Koeppenkastrop, D., De Carlo, E.H.. 1992. Sorption of rare-earth elements from
580 seawater onto synthetic mineral particles: An experimental approach. Chemical
581 Geology, 95(3-4), 251-263.
582 Koeppenkastrop, D., De Carlo, E.H. 1993. Uptake of rare earth elements from
583 solution by metal oxides. Environmental Science & Technology, 27(9),
584 1796-1802.
585 Lee, J.H., Byrne, R.H., 1992. Examination of comparative rare earth element
586 complexation behavior using linear free-energy relationships. Geochimica et
587 Cosmochimica Acta 56, 1127-1137.
588 Liu, H.Y., Guo, H.M., Xing, L.N., Zhan, Y.H., Li, F.L., Shao, J.L., N, H., L, X., Li,
589 C.Q. 2016. Geochemical behaviors of rare earth elements in groundwater along a
590 flow path in the North China Plain. Journal of Asian Earth Sciences, 117, 33-51.
591 Livingstone, D.A. 1963. Chemical composition of rivers and lakes. US Government
592 Printing Office.
593 Luo, Y.R., Byrne, R.H. 2001. Yttrium and rare earth element complexation by
594 chloride ions at 25 C. Journal of Solution Chemistry, 30(9), 837-845.
595 Luo, Y., Millero, F.J. 2004. Effects of temperature and ionic strength on the stabilities
596 of the first and second fluoride complexes of yttrium and the rare earth
597 elements. Geochimica et cosmochimica acta, 68(21), 4301-4308.
598 Luo, Y.R., Byrne, R.H., 2004. Carbonate complexation of yttrium and the rare earth
599 elements in natural rivers. Geochimica et Cosmochimica Acta 68, 691-699.
600 Mathur, S.S., Dzombak, D.A., 2006. Chapter 16-surface complexation modeling:
601 goethite. In: Johannes, L. (Ed.), Interface Science and Technology. 11. Elsevier,
602 pp. 443-468.

603 Millero, F.J., 1992. Stability constants for the formation of rare earth inorganic
604 complexes as a function of ionic strength. Geochimica et Cosmochimica Acta
605 56, 3123-3132.
606 Nakada, R., Takahashi, Y., Tanimizu, M. 2013. Isotopic and speciation study on
607 cerium during its solid–water distribution with implication for Ce stable isotope
608 as a paleo-redox proxy. Geochimica et Cosmochimica Acta, 103, 49-62.
609 Noack, C.W., Dzombak, D.A., Karamalidis, A.K., 2014. Rare earth element
610 distributions and trends in natural waters with a focus on groundwater.
611 Environmental Science & Technology 48, 4317-4326.
612 Nordstrom, D.K., Plummer, L.N., Langmuir, D., Busenberg, E., May, H.M., Jones,
613 B.F., Parkhurst, D.L. 1990. Revised chemical equilibrium data for major
614 water-mineral reactions and their limitations.
615 Ohta, A., Kawabe, I. 2001. REE (III) adsorption onto Mn dioxide (δ-MnO_2) and Fe
616 oxyhydroxide: Ce (III) oxidation by δ-MnO_2. Geochimica et Cosmochimica
617 Acta, 65(5), 695-703.
618 Parkhurst, D.L., Appelo, C. A.J. 2013. Description of input and examples for
619 PHREEQC version 3-a computer program for speciation, batch-reaction,
620 one-dimensional transport, and inverse geochemical calculations. US geological
621 survey techniques and methods, book, 6, 497.
622 Pourret, O., Davranche, M., Gruau, G., Dia, A., 2007. Rare earth elements
623 complexation with humic acid. Chemical Geology, 243, 128-141.
624 Pourret, O., Martinez, R.E. 2009. Modeling lanthanide series binding sites on humic
625 acid. Journal of colloid and interface science, 330(1), 45-50.
626 Pourret, O., Gruau, G., Dia, A., Davranche, M., Molenat, J. 2010. Colloidal control on
627 the distribution of rare earth elements in shallow groundwaters. Aquatic
628 Geochemistry, 16(1), 31.
629 Pourret, O., Davranche, M. 2013. Rare earth element sorption onto hydrous
630 manganese oxide: A modeling study. Journal of Colloid and Interface
631 Science, 395, 18-23.

Pourret, O., Tuduri, J. 2017. Continental shelves as potential resource of rare earth elements. Scientific Reports, 7.

Quinn, K.A., Byrne, R.H., Schijf, J. 2006. Sorption of yttrium and rare earth elements by amorphous ferric hydroxide: influence of solution complexation with carbonate. Geochimica et Cosmochimica Acta, 70(16), 4151-4165.

Quinn, K.A., Byrne, R.H., Schijf, J. 2007. Sorption of yttrium and rare earth elements by amorphous ferric hydroxide: influence of temperature. Environmental Science & Technology, 41(2), 541-546.

Rim, K.T., Koo, K.H., Park, J.S. 2013. Toxicological evaluations of rare earths and their health impacts to workers: a literature review. Safety and health at work, 4(1), 12-26.

Shannon, R.T. 1976. Revised effective ionic radii and systematic studies of interatomic distances in halides and chalcogenides. Acta crystallographica section A: crystal physics, diffraction, theoretical and general crystallography, 32(5), 751-767.

Schindler, P.W., Fürst, B., Dick, R., Wolf, P.U. 1976. Ligand properties of surface silanol groups. I. Surface complex formation with Fe^{3+}, Cu^{2+}, Cd^{2+}, and Pb^{2+}. Journal of Colloid and Interface Science, 55(2), 469-475.

Schijf, J., Byrne, R.H. 2004. Determination of SO_4 β_1 for yttrium and the rare earth elements at I=0.66 m and t=25 ºC-implications for YREE solution speciation in sulfate-rich waters. Geochimica et cosmochimica acta, 68(13), 2825-2837.

Schijf, J., Marshall, K.S. 2011. YREE sorption on hydrous ferric oxide in 0.5 M NaCl solutions: a model extension. Marine Chemistry, 123(1), 32-43.

Schott, J., Pokrovsky, O.S., Oelkers, E.H. 2009. The link between mineral dissolution/precipitation kinetics and solution chemistry. Reviews in mineralogy and geochemistry, 70(1), 207-258.

Tang, J., Johannesson, K.H. 2003. Speciation of rare earth elements in natural terrestrial waters: assessing the role of dissolved organic matter from the modeling approach. Geochimica et Cosmochimica Acta, 67(13), 2321-2339.

661 Tang, J., Johannesson, K.H. 2005. Adsorption of rare earth elements onto Carrizo
662 sand: experimental investigations and modeling with surface
663 complexation. Geochimica et Cosmochimica Acta, 69(22), 5247-5261.
664 Tonkin, J.W., Balistrieri, L.S., Murray, J.W. 2004. Modeling sorption of divalent
665 metal cations on hydrous manganese oxide using the diffuse double layer
666 model. Applied Geochemistry, 19(1), 29-53.
667 Verplanck, P.L., Nordstrom, D.K., Taylor, H.E., Kimball, B.A. 2004. Rare earth
668 element partitioning between iron oxyhydroxides and acid mine waters. Applied
669 Geochemistry19, 1339-1354.
670 Verplanck, P.L., Furlong, E.T., Gray, J.L., Phillips, P.J., Wolf, R.E., Esposito, K.
671 2010. Evaluating the behavior of gadolinium and other rare earth elements
672 through large metropolitan sewage treatment plants. Environmental Science &
673 Technology, 44(10), 3876-3882.
674 Wood, S.A. 1990. The aqueous geochemistry of the rare-earth elements and yttrium:
675 1. Review of available low-temperature data for inorganic complexes and the
676 inorganic REE speciation of natural waters. Chemical Geology, 82, 159-186.
677 Zhu, W.F., Xu, S.Q., Shao, P.P., Zhang, H., Wu, D.S., Yang, W.J., Feng, J., Feng, L.
678 2005. Investigation on liver function among population in high background of
679 rare earth area in South China. Biological trace element research, 104(1), 1-7.

Table1 SCM parameters for iron oxyhydroxide (The pK values are taken from Dzobmbak and Morel (1990); the site densities and specific surface area are from Parkhurst and Appelo (2013)).

pK_{a1}	pK_{a2}	Specific surface area (m^2/mol)	Total site density (mol/mol Fe)	Strong site density ($\equiv Fe^sOH$) (mol/mol Fe)	Weak site density ($\equiv Fe^wOH$) (mol/mol Fe)
7.29	8.93	100000	0.101	0.001	0.1

Table 2 Stability constants extrapolated from the LFER

REE	$\log K_{LnOH}$	$\log K_{Ln(OH)2}$	$\log K_{Ln(OH)3}$	$\log K_{\equiv Fe^{s}OLn}$	$\log K_{\equiv Fe^{w}OLn}$
La	5.19	-4.14	-13.9	1.68	-1.16
Ce	5.66	-3.6	-13.23	2.22	-0.54
Pr	5.68	-3.27	-12.63	2.25	-0.52
Nd	5.82	-3.04	-12.4	2.41	-0.33
Sm	6.16	-2.51	-11.91	2.81	0.11
Eu	6.24	-2.37	-11.41	2.90	0.21
Gd	6.17	-2.37	11.72	2.82	0.12
Tb	6.36	-2.18	-11.08	3.04	0.37
Dy	6.41	-2.1	-10.83	3.10	0.43
Ho	6.44	-2.07	-10.56	3.13	0.47
Er	6.48	-1.96	-10.35	3.18	0.52
Tm	6.61	-1.88	-10.18	3.33	0.69
Yb	6.76	-1.74	-9.85	3.51	0.89
Lu	6.73	-2.67	-9.85	3.47	0.85

Fig. 1

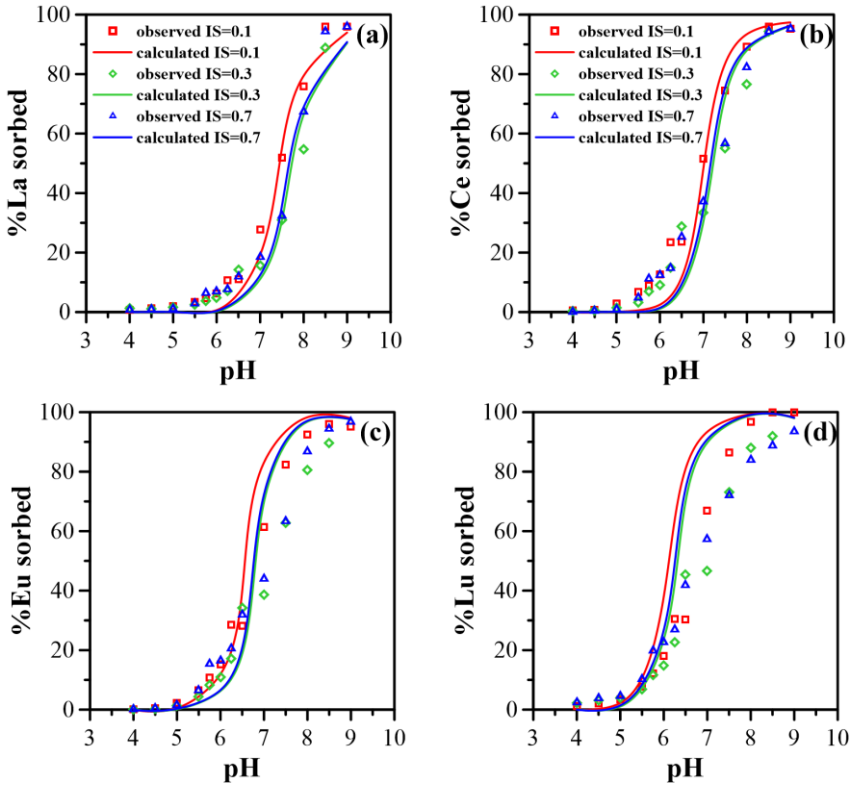

Figure 1 A comparison between the experimental and calculated proportion of sorbed La, Ce, Eu and Lu with the extrapolated stability constants under the experimental conditions documented by De Carlo et al. (1998). The dots correspond to the experimental data, and the solid lines correspond to the model fit ((a): La; (b): Ce; (c): Eu; (d): Lu).

Fig. 2

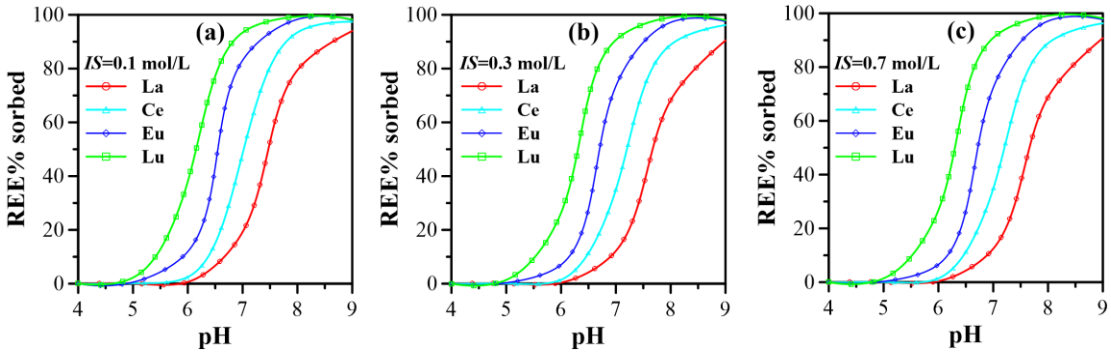

Figure 2 Proportion of REE ([REE]=125 μg/L) sorbed to iron oxyhydroxide (total [Fe(III)] = 10 mg/L) as a function of pH at various IS: (a) 0.1 mol/L, (b) 0.3 mol/L and (c) 0.7 mol/L.

Fig. 3

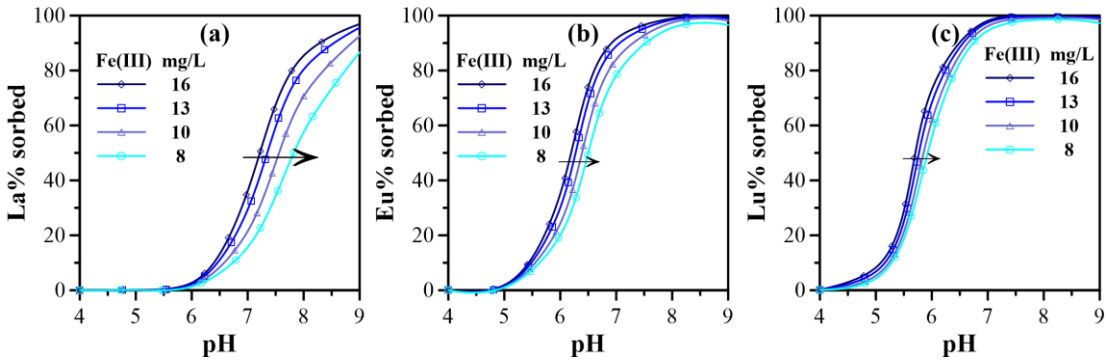

Figure 3 pH edges for REE sorption ((a): La; (b): Eu; (c): Lu; [REE]=125 µg/L; IS=0.5 mol/L). Arrows indicate decreasing iron oxyhydroxide concentration.

Fig. 4

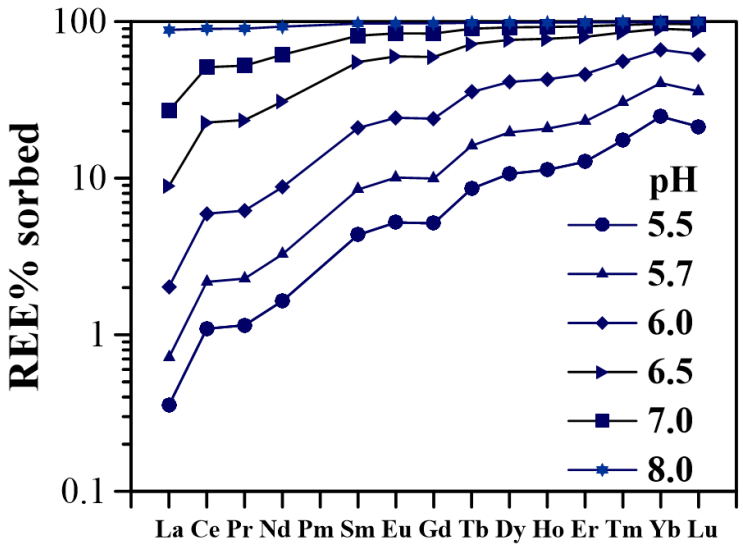

Figure 4 Patterns arising from the calculated proportion of sorbed REE under the experimental conditions described by De Carlo et al. (1998) (IS = 0.5 mol/L).

Fig. 5

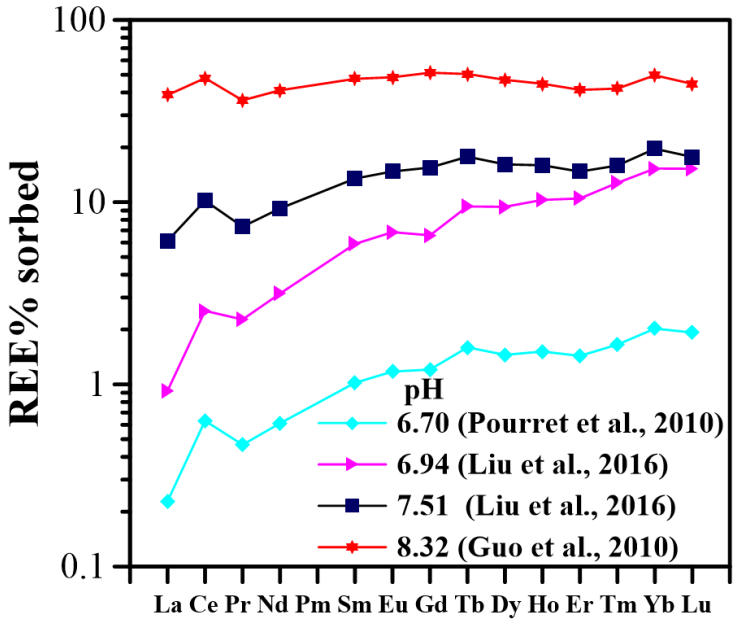

Figure 5 Modeling calculation with literature data from the field studies including Pourret et al. (2010) (sample PG3), Guo et al. (2010) (No. well 48) and Liu et al. (2016) (sampling location at a distance of 0 km and 61 km from the recharge area, respectively; for detailed information see Liu et al. (2016)).

Fig. 6

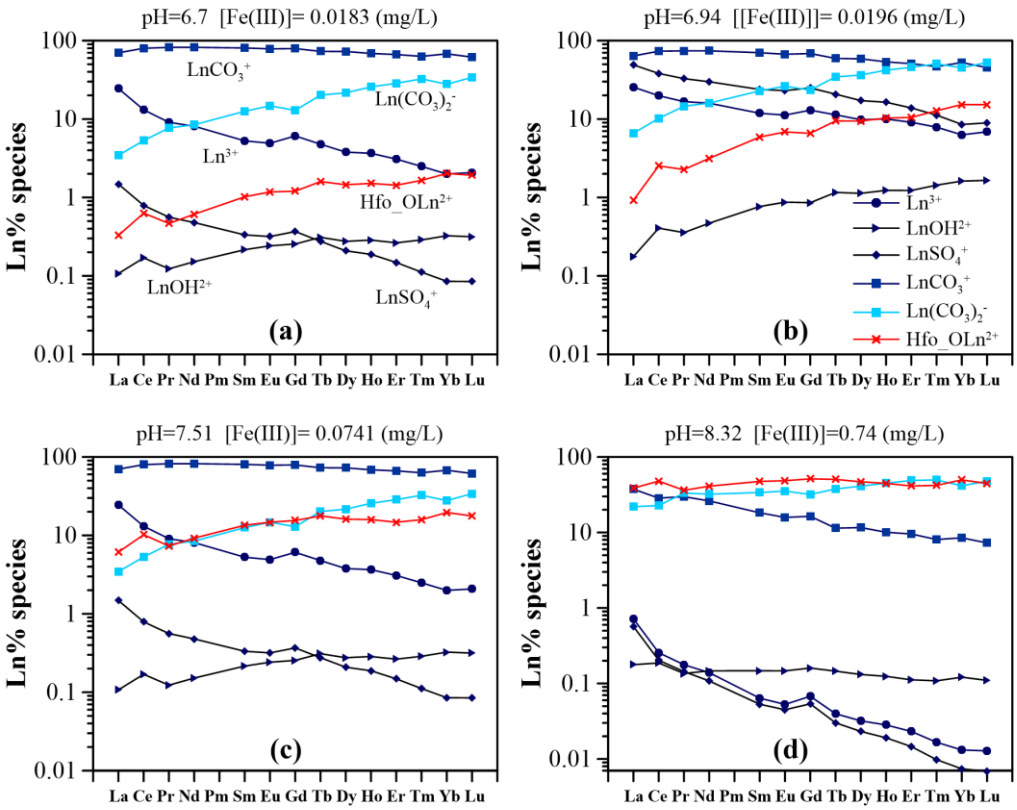

Figure 6 Results of REE speciation calculation for groundwater samples ((a): Pourret et al., (2010) (sample PG3); (b) and (c): Liu et al., (2016) (sampling location at a distance of 0 km and 61 km from the recharge area, respectively); (d): Guo et al., (2010) (No. well 48)).

Fig. 7

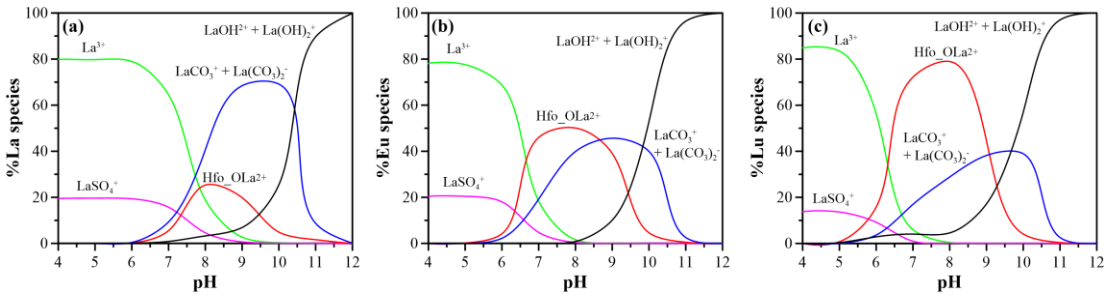

Figure 7 Speciation of (a) La, (b) Eu, and (c) Lu in groundwater with [Fe(III)] of 0.672 mg/L as a function of pH (Concentrations of the major anions and REE from Wood (1990); concentrations of the major cations and Fe from Livingstone (1963)) It must be noted that the minor fluoride, chloride and nitrate complexes (below < 1%) are not presented for clarity.

Supplementary Information for

Rare earth elements sorption to iron oxyhydroxide: model development and application to groundwater

Haiyan Liu[1, 2, 3], Olivier Pourret[3,*], Huaming Guo[1, 2], Jessica Bonhoure[3]

[1]State Key Laboratory of Biogeology and Environmental Geology, China University of Geosciences (Beijing), Beijing 100083, P.R. China

[2]MOE Key Laboratory of Groundwater Circulation & Environment Evolution & School of Water Resources and Environment, China University of Geosciences (Beijing), Beijing 100083, P.R. China

[3]UniLaSalle, HydrISE, *60026 Beauvais Cedex*, France

Contents of this file

Table S1 Stability constants (log k) for REE inorganic anion complexation

	La	Ce	Pr	Nd	Sm	Eu	Gd	Tb	Dy	Ho	Er	Tm	Yb	Lu
$REE(OH)^{2+}$	-8.81	-8.34	-8.32	-8.18	-7.84	-7.76	-7.83	-7.64	-7.59	-7.56	-7.52	-7.39	-7.24	-7.27
$REE(OH)_2^{+}$	-18.14	-17.6	-17.27	-17.04	-16.51	-16.37	-16.37	-16.18	-16.1	-16.07	-15.96	-15.88	-15.74	-16.67
$REE(OH)_3$ (aq)	-27.9	-27.23	-26.63	-26.4	-25.91	-25.41	-2.28	-25.08	-24.83	-24.56	-24.35	-24.18	-23.85	-23.85
$REE(CO_3)^{+}$	6.73	7.06	7.23	7.28	7.46	7.48	7.39	7.46	7.56	7.55	7.61	7.68	7.81	7.75
$REE(CO_3)_2^{-}$	11.3	11.76	12.08	12.17	12.53	12.63	12.48	12.78	12.91	13	13.12	13.27	13.3	13.37
$REE(NO_3)^{2+}$	0.58	0.69	0.69	0.79	0.78	0.83	0.47	0.51	0.15	0.25	0.15	0.2	0.25	0.56
$REE(SO_4)^{+}$	3.61	3.61	3.62	3.6	3.63	3.64	3.61	3.59	3.57	3.54	3.51	3.48	3.46	3.44
$REEF^{+2}$	3.63	3.85	3.86	3.82	4.14	4.26	4.23	4.36	4.39	4.28	4.27	4.28	4.37	4.24
$REECl^{+2}$	0.74	0.68	0.71	0.71	0.67	0.69	0.71	0.67	0.7	0.71	0.7	0.71	0.69	0.67
$REECl_2^{+}$	0.51	0.46	0.45	0.47	0.42	0.44	0.46	0.43	0.43	0.45	0.45	0.46	0.44	0.43

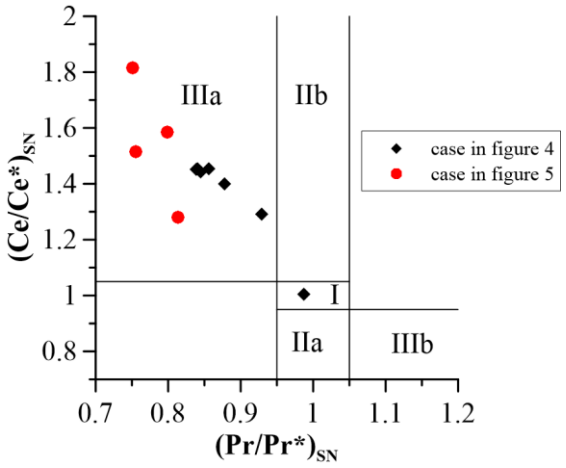

Figure S2 The calculated Ce/Ce* and Pr/Pr * for cases shown in figure 4 and 5. Field I: neither Ce nor La anomaly; field IIa: positive La anomaly, no Ce anomaly; field IIb: negative La anomaly, no Ce anomaly; field IIIa: positive Ce anomaly; field IIIb: negative Ce anomaly. For further explanation see Bau and Dulski. (1996). (The only sample located in area I is the case with IS=0.5 and pH=8, where nearly all of the REEs are sorbed onto solid phase (see figure 4 in the text))